ORIGINAL PAPER

Electronic Properties of Novel Materials

physica status solidi b

www.pss-b.com

High-Resolution Nanospectroscopy of Boron Nitride Nanotubes

Dániel Datz, Gergely Németh, Hajnalka M. Tóháti, Áron Pekker, and Katalin Kamarás*

Scattering type scanning near-field optical microscopy (s-SNOM) is an effective tool for the nanoscale examination of nano-objects. In this paper, we present a modified device setup that enables spectroscopic measurements with a tunable laser, even without an FTIR (Fourier Transform Infrared) spectroscopy add-on. We demonstrate the effectiveness of this setup by measurements on boron nitride nanotubes (BNNTs). In far-field absorption measurements, BNNTs have a characteristic peak around 1375 cm^{-1} due to a phonon polariton mode. This peak is also visible in near-field measurements along with several other peaks that are not present in the far-field spectrum. As these peaks are caused by local defects, their spatial distribution reveals the defect structure of individual nanotubes.

1. Introduction

Scattering type near-field optical microscopy (s-SNOM) is an effective tool to create optical maps of nano-objects. The high spatial resolution is achieved by utilizing the near-field interaction between a substrate and an illuminated, metal-coated AFM (atomic force microscope) tip serving as a nanoantenna. Since the spatial resolution of such maps is limited only by the radius of the AFM tip (up to 10 nm), the s-SNOM method is especially useful for optical mapping of single nano-objects whose dimensions are below the Abbe limit.[1] The near-field method was successfully used to observe collective excitations in graphene,[2] topological insulators,[3] carbon and boron nitride nanotubes[4,5] and spatial or temporal material variations in black phosphorus[6] and different kinds of alloys.[7]

Besides spatial variations at a single wavelength, obtaining a spectrum over a wider frequency range is equally important. Here we present a solution for a multi-frequency scanning measurement setup, using a tunable infrared (IR) laser. Its effectiveness is showcased with measurements on multi-walled boron nitride nanotubes and mapping their defect structure.

D. Datz, G. Németh, H. M. Tóháti, Dr. Á. Pekker, Prof. K. Kamarás
Institute for Solid State Physics and Optics, Wigner Research Centre for Physics, Hungarian Academy of Sciences, 1121 Budapest, Hungary
E-mail: datz.daniel@wigner.mta.hu

DOI: 10.1002/pssb.201700277

2. Experimental Methods

Purified boron nitride nanotubes were acquired from the group of Andrei Khlobystov (University of Nottingham) as white powder.[9] The powder was dissolved in isopropanol by ultrasonication for 5 h, creating a suspension of approximately 1 m/m%. This suspension was either spincoated (2500 rpm, 60 s) or dropcasted upon a clean Si substrate. The sample prepared this way consists of separated BNNTs throughout its surface, making the AFM measurements straightforward. A map of a typical multi-walled BNNT is presented in **Figure 1**.

The s-SNOM device (Neaspec GmbH[10]) is composed of an AFM and an optical apparatus (lasers and mirrors) that properly illuminates the metal-coated AFM tip. The incident radiation causes a near-field interaction between the AFM tip and the studied object. When the thickness of the inspected object is in the order of a few nanometers, the substrate also participates in the interaction. Thus substrate-enhanced scattering can also be achieved.[11] The optical information is then carried by the scattered electromagnetic radiation to an MCT detector (**Figure 2**).

Modifying the s-SNOM setup for spectroscopic measurements requires two steps. First the computer control of the illuminating laser has to be set up. The laser controller is able to communicate with a computer through a GPIB port. Communication and remote control of the tunable laser was achieved by a dedicated Labview program.

The second step is properly setting the modulation amplitude of the vibrating mirror. Our s-SNOM device uses the pseudo-heterodyne detection method to minimize the amount of background scattering coming from sources other than the near-field interaction. In the pseudo-heterodyne detection,[8] the weak near-field signal is amplified by a reference beam that is phase-modulated by a vibrating mirror. Since the detected signal is the intensity of the incident electromagnetic field on the detector, this produces an output signal with a component that is periodic in both the AFM tip vibration (Ω) and the mirror vibration (M). This means that the Fourier transform of the detected output signal has peaks at frequencies $n\Omega + mM$ where n and m are integers.

The optical amplitude (s_2) and phase (ϕ_2) are calculated from peaks $C_{2,1}$ and $C_{2,2}$ ($n = 2$, $m = 1,2$) as follows:

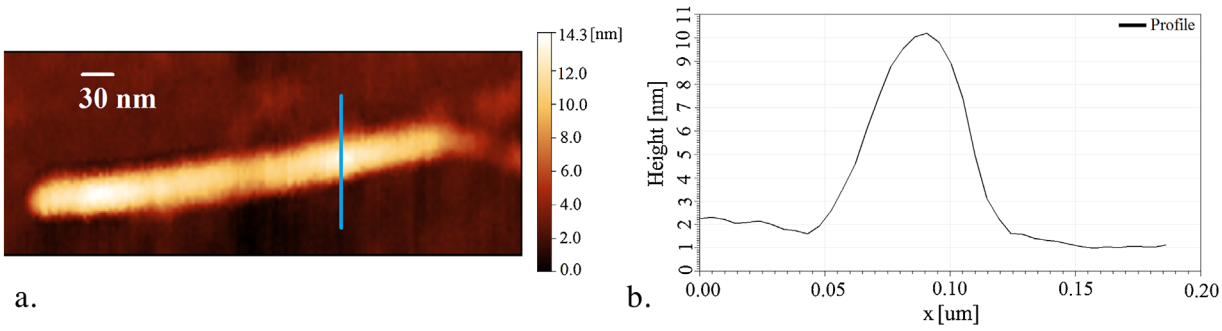

Figure 1. a) AFM topography image of an individual multi-walled boron nitride nanotube. The blue line indicates a cross-section along which the height profile (shown on b) was taken.

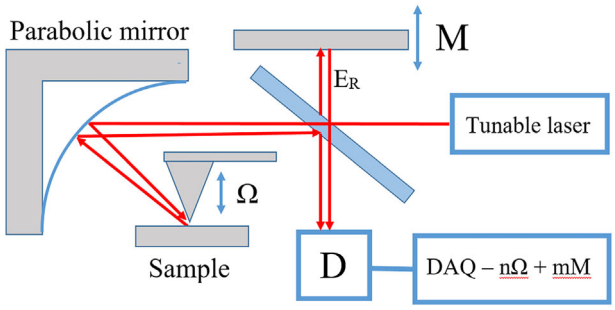

Figure 2. Schematic diagram of the s-SNOM device. The reference beam (E_R) is phase modulated in a Michelson interferometer (D – detector, DAQ – Data Acquisition Board). This detection technique is called the pseudo-heterodyne detection method.[8]

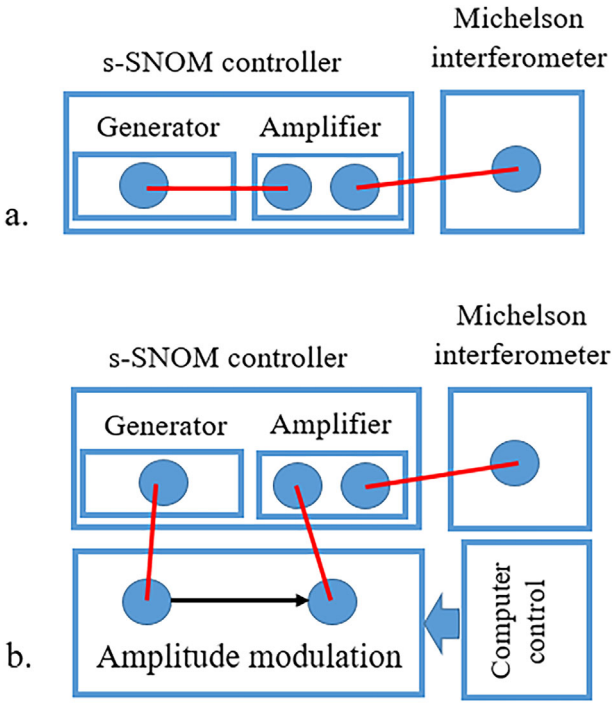

Figure 3. a) The original setup of the s-SNOM device. b) The modified setup.

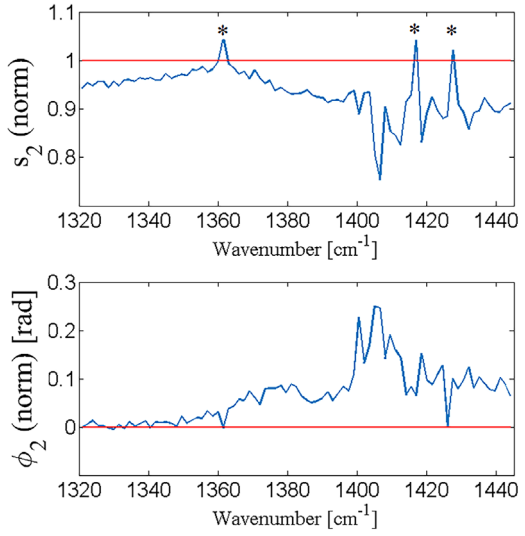

Figure 4. Measured optical ($n = 2$, $m = 1,2$) amplitude and phase contrast spectra according to Eqs. (1) and (2), normalized to the silicon surface (Eqs. (6) and (7)). The red lines represent the zero contrast values. The observed spikes marked by asterisks were caused by water absorption.

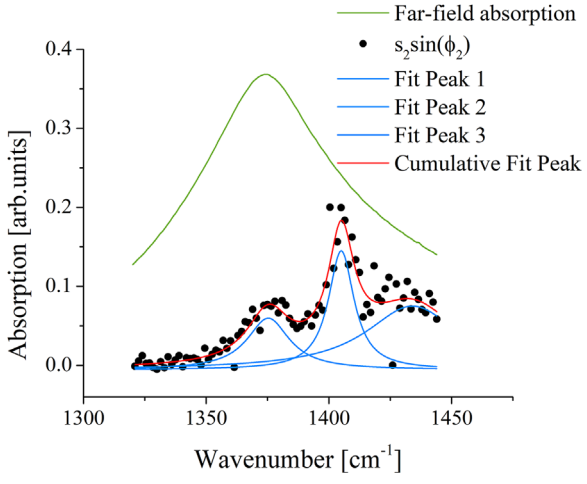

Figure 5. Far-field and near-field infrared absorption of boron nitride nanotube. The near-field absorption values were calculated according to Eqs. (6)–(8).

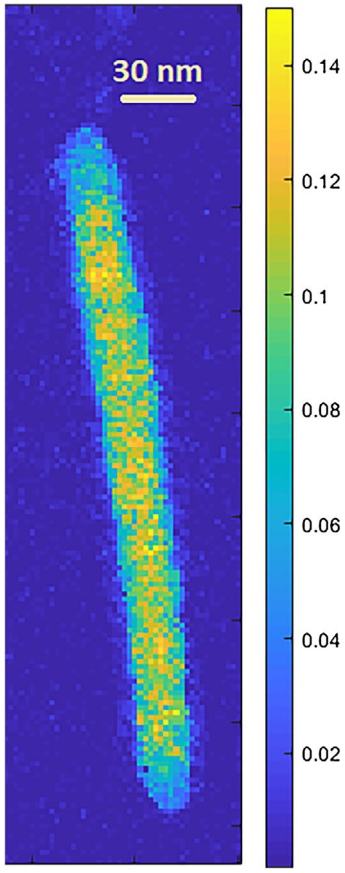

Figure 6. Absorption values along an individual multi-walled BNNT at 1375 cm^{-1}. The absorption is relatively uniform along the nanotube, without large deviations.

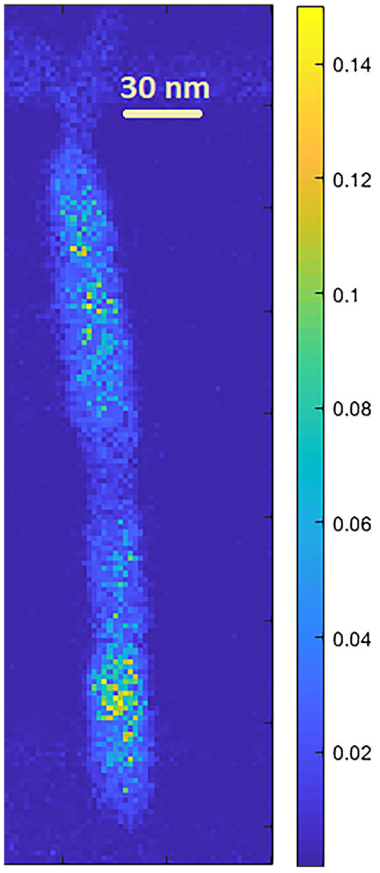

Figure 7. Absorption values along an individual multi-walled BNNT at 1430 cm^{-1}. The absorption is highly position dependent.

$$s_2 = \sqrt{|C_{2,1}|^2 + |C_{2,2}|^2}, \tag{1}$$

$$\phi_2 = \arctan\frac{|C_{2,1}|}{|C_{2,2}|}. \tag{2}$$

The amplitude and the phase become independent when the vibrating mirror amplitude is set correctly. This is a consequence of the fact that the measured electromagnetic field is periodic in frequency M:

$$E = \sum_{m=-\infty}^{\infty} \rho_m e^{imMt} \tag{3}$$

where

$$\rho_m \propto J_m(\gamma) e^{i\Psi_R + im\pi/2} \tag{4}$$

where Ψ_R is the phase offset caused by the optical path difference between the two arms of the Michelson interferometer. Since

$$C_{n,m} \propto \sigma_{T,n}\rho_m^* + \sigma_{T,n}\rho_m, \tag{5}$$

where $\sigma_{T,n}$ is the nth component of the total scattering cross-section σT, $C_{n,m}$ is also proportional to the mth Bessel function $J_m(\gamma)$ where γ is the so-called modulation depth, related to the amplitude of the vibrating mirror: $\gamma = 2\frac{2\pi}{\lambda}A_{mirror}$ where λ is the wavelength and A_{mirror} is the amplitude of the vibration. Calculation of the optical amplitude and phase is the simplest if the modulation depth is set so that $J_1(\gamma) = J_2(\gamma)$, which yields $\gamma = 2.63$.

Since the modulation depth is dependent on the wavelength, this means that it has to be reset at every wavenumber. This is achieved by controlling the piezo actuator of the vibrating mirror. In the original setup a built-in signal generator produces the sinusoid signal of the mirror with the correct frequency, which is then amplified to the 150 V piezo driving signal. In our setup, we use a signal generator (Stanford Research DS345) for amplitude modulation of the generator signal. By remote controlling the signal generator by the same Labview program mentioned above, we can control the piezo signal and thereby the amplitude of the vibrating mirror. A simplified diagram of the setup is presented in **Figure 3**b.

3. Results and Discussion

The infrared spectrum was taken across several line sections along a single boron nitride nanotube in the wavenumber range

1320–1440 cm^{-1} (only limited by the capabilities of our laser), with 2 cm^{-1} step (**Figure 4**). The optical data of the nanotube can be interpreted only as contrast respective to the substrate. The contrast amplitude and phase can be calculated from the optical data acquired when the tip is on top of the nanotube ($s_{2,tube}$ and $\phi_{2,tube}$) and when it is at a distance from it, on the substrate ($s_{2,subs}$ and $\phi_{2,subs}$) as

$$s_{2,norm} = \frac{s_{2,tube}}{s_{2,subs}} \tag{6}$$

and

$$\phi_{2,norm} = \phi_{2,tube} - \phi_{2,subs}. \tag{7}$$

From the acquired optical amplitude and phase ($n = 2$, $m = 1,2$), absorption values are calculated as follows:

$$A = s_2 \sin \phi_2. \tag{8}$$

The calculated absorption spectrum across every section shows a characteristic peak around 1375 cm^{-1}, in very good agreement with the far-field absorption measurements, and is attributed to a phonon polariton mode (**Figure 5**).[12] This peak is present at every position along the nanotube as shown in **Figure 6**.

Additional peaks are also observable, but both the intensity and the position of these peaks are very strongly dependent on the position of the tip along the nanotube. The strong position-dependent behavior of these artifacts suggests that they are connected to local defect modes due to scattering on surface defects. This defect structure of the examined BNNT is presented in **Figure 7**.

It is expected that the defects are mainly introduced by the purification and opening procedure of the nanotubes, thereby located mainly on the outermost tubes. Since the near-field penetrates into the multi-walled nanotubes several tens of nanometers deep, it is not possible to map the defect structure of the outermost tube until a single-walled sample is available. Although near-field tomography is capable of determining the subsurface structure of certain samples,[13] in this case the radii of the nanotubes are too small for the reliable application of the method.

4. Conclusion and Outlook

We showed that spectroscopic measurements with a near-field microscope are possible with modification of the measurement setup. We presented measurements on multi-walled boron nitride nanotubes, on which we were able to detect the characteristic phonon polariton peak around 1375 cm^{-1}. Furthermore, we showed that it is possible to map the defect structure of the multi-walled BNNTs which shows the distribution of the local defect modes. It is an interesting question whether the different layers of tubes can be distinguished or if there is interaction between the layers of the multi-walled tubes. The answer will be possible to obtain if the signal-to-noise ratio can be further improved with the development of the measurement setup.

Acknowledgements

The purified BNNT sample was provided by Kate Walker and Graham Rance from the University of Nottingham. Research was supported by the Hungarian National Research Fund (OTKA) no. SNN 118012. Á.P. gratefully acknowledges support from the János Bolyai Fellowship of the Hungarian Academy of Sciences and from the National Research, Development and Innovation Office - NKFIH PD 121320.

Conflict of Interest

The authors declare no conflict of interest.

Keywords

absorption spectra, BN, nanotubes, near-field infrared microscopy, scanning near-field optical microscopy

Received: June 7, 2017
Revised: August 10, 2017
Published online: September 26, 2017

[1] T. Taubner, F. Keilmann, R. Hillenbrand, *J. Korean Phys. Soc.* **2005**, *47*, 213.
[2] Z. Fei, A. Rodin, G. Andreev, W. Bao, A. McLeod, M. Wagner, L. Zhang, Z. Zhao, M. Thiemens, G. Dominguez, G. Dominguez, M. Thiemens, M. Fogler, A. Castro-Neto, C. Lau, F. Keilmann, D. Basov, *Nature* **2012**, *487*, 82.
[3] A. M. Dubrovkin, G. Adamo, J. Yin, L. Wang, C. Soci, Q. J. Wang, N. I. Zheludev, *Adv. Opt. Mater.* **2017**, *5*, 1600768.
[4] G. Németh, D. Datz, H. M. Tóháti, Á. Pekker, K. Kamarás, *Phys. Status Solidi B* **2016**, *253*, 2413.
[5] X. G. Xu, B. G. Ghamsari, J. H. Jiang, L. Gilburd, G. O. Andreev, C. Zhi, Y. Bando, D. Golberg, P. Berini, G. C. Walker, *Nature Commun.* **2014**, *5*, 4782.
[6] S. Gamage, Z. Li, V. S. Yakovlev, C. Lewis, H. Wang, S. B. Cronin, Y. Abate, *Adv. Mater. Interfaces* **2016**, *3*, 1600121.
[7] M. Takahashi, A. Moto, S. Tanaka, T. Tanabe, S. Takagishi, K. Karatani, M. Nakayama, K. Matsuda, T. Saiki, *J. Cryst. Growth* **2000**, *221*, 461.
[8] N. Ocelic, A. Huber, R. Hillenbrand, *App. Phys. Lett.* **2006**, *89*, 101124.
[9] K. E. Walker, *PhD Thesis*, University of Nottingham, Unpublished.
[10] Neaspec GmbH, http://www.neaspec.com (accessed: August 2017).
[11] A. Cvitkovic, N. Ocelic, R. Hillenbrand, *Nano Lett.* **2007**, *7*, 3177.
[12] B. G. Ghamsari, X. G. Xu, L. Gilburd, G. C. Walker, P. Berini, *J. Optics – UK* **2014**, *16*, 114008.
[13] J. Sun, J. C. Schotland, R. Hillenbrand, P. S. Carney, *Appl. Phys. Lett.* **2009**, *95*, 121108.